Japanese Journal of Applied Physics

The Japan Society of Applied Physics

REGULAR PAPER • OPEN ACCESS

Understanding of relationship between dopant and substitutional site to develop novel phase-change materials based on In_3SbTe_2

To cite this article: Minho Choi *et al* 2019 *Jpn. J. Appl. Phys.* **58** SBBB02

OPEN ACCESS

Japanese Journal of Applied Physics **58**, SBBB02 (2019) **REGULAR PAPER**

https://doi.org/**10.7567/1347-4065/aafa6a**

Understanding of relationship between dopant and substitutional site to develop novel phase-change materials based on In_3SbTe_2

Minho Choi[1], Heechae Choi[2], Jinho Ahn[3*], and Yong Tae Kim[1*]

[1]*Semiconductor Materials and Device Laboratory, Korea Institute of Science and Technology, Seoul 02792, Republic of Korea*
[2]*Institute of Inorganic Chemistry, University of Cologne, Cologne 50939, Germany*
[3]*Division of Materials Science and Engineering, Hanyang University, Seoul 04763, Republic of Korea*

[*]E-mail: ytkim@kist.re.kr; jhahn@hanyang.ac.kr

Received October 1, 2018; accepted December 11, 2018; published online February 4, 2019

For over a decade, phase-change materials have been widely researched using various materials and methods. Despite efforts, the design of novel materials is nowhere near reported. In this paper, we provide the data for doping in In_3SbTe_2 material with doping formation energy and distortion angle at In, Sb, and Te sites. Information on the 29 dopants reduces unnecessary time cost to select the dopant for the IST material since the dopant with the positive and big formation energy should be excluded. In addition, excessive dopants disturb the stable phase transition, for this reason, the approximate limit of concentration for doping is suggested with experimental results through XRD, TEM, and electrical characteristics. This study gives one guideline of the many methods to develop and discover the novel materials in terms of substitutional site and the amount of dopant. © 2019 The Japan Society of Applied Physics

1. Introduction

Phase-change material (PCM) is one of the core parts of non-volatile phase-change random access memory (PRAM) devices because the phases of PCMs are reversibly changed between the amorphous phase (high resistance state) and crystalline phase (low resistance state) and even make many intermediate states through fast-speed electrical pulses.[1–4)] To use PRAM for the various applications, low-power consumption as well as high speed are also absolutely considered as the vital factor to commercialize.[5,6)] Faster speed and lower power consumption directly correspond to the faster phase transition and amorphization of the PCMs since the repeated operation of unstable materials will lead to problems such as phase separation and segregation.[7,8)] Over a decade, although most research has been dominantly devoted to $Ge_2Sb_2Te_5$ material,[9–14)] there is a limit to the further improvement on inherent properties of the GeSbTe system for low-power memory and neuromorphic devices. Therefore, other materials such as InSbTe,[15–18)] AgInSbTe,[19,20)] and SbTe[21,22)] systems are required to improve the properties.[23–27)] Then, the key point to developing novel PCMs is to investigate local distortion effects in these materials.[28–30)] According to the previous work on In_3SbTe_2 (IST),[31)] the "set" and "reset" speed could be improved by Bi doping. Through the combination of systematic high-resolution transmission electron microscopy (HRTEM) analysis and density functional theory (DFT) calculations, it was found that Bi dopant makes lattice distortions by $\sim 2^{\circ}$ of the crystalline phase of IST and the crystalline IST is thermodynamically stable even with the lattice distortion from the calculated negative doping energy of Bi at the Sb site. From these results, it is predictable that the lattice distortion by the dopant can improve the speed and power consumption as well as the thermal stability. The computational high-throughput screening of dopants by DFT was essential for selecting an ideal dopant to satisfy the large lattice distortions and the thermodynamic stability because it was almost impossible to experimentally test all of the elements in the periodic table.[32)] For this reason, in our previous study,[33)] two criterions were considered to choose a proper doping element for the IST: (i) the element is doped into the IST atomic structure with thermodynamic stability, and (ii) the element offers largest lattice distortion after the substitutional doping. In the study, the properties of 29 elements as dopants in IST material are analyzed in terms of thermal stability and distortion angle at particular site among In, Sb, and Te. That is why the objective of the work is to choose the most reasonable dopant and analyze the doped IST. However, to help understand the dopant of IST for future work and not to unnecessarily carry out the same work, all data of doping formation energy and distortion angle at all sites are reported in this paper. Besides, the importance of the doping site is discussed, having not been considered previously.

2. Experimental methods

DFT[34,35)] calculations were performed using the generalized gradient approximation and Perdew–Burke–Ernzerhof parameterization.[36,37)] We employed the Vienna ab initio simulation package program.[38)] In our DFT calculations, Kohn–Sham orbitals were expanded with a cutoff energy of 400.0 eV, and a $2 \times 2 \times 2$ equally spaced k-point grids were used for the Brillouin zone sampling.[39)] The supercell volume and all atoms were fully relaxed. The dimension of IST supercell was fixed at 12.435 Å and the time step of AIMD was 1 fs.

Twenty-nine dopants (Ag, Bi, Co, Cr, Er, Fe, Ga, Gd, Ir, Po, Rh, Ge, Ta, Nb, Sc, Zr, Mo, Si, La, Lu, Tl, V, Pr, Tb, Y, Yb, Cu, Ti, and Zn) were calculated by. The doping energy of metal ions into IST crystal (ΔE_f) was obtained using this Eq. (1):

$$\Delta E_f = E_{\mathrm{IST:D}} - E_{\mathrm{IST}} - E_{\mathrm{D}} + E_0, \quad (1)$$

where $E_{\mathrm{IST:D}}$, E_{IST}, E_{D}, and E_0 are, respectively, the calculated total energy of the doped IST, pure IST supercells, pure solid dopant, and pure solid of the removed host ion.

The Bi-doped IST (Bi-IST) and Y-doped IST (Y-IST) thin films were co-sputtered using bismuth, yttrium and IST targets. The sputtering processes were performed in an Ar atmosphere (5 mTorr). The PRAM were fabricated with contact area of 250 nm × 250 nm. The cross-sectional structure is consisted of Ti/TiN (top electrode)/PCM/W (heater)/TiN/Ti (bottom electrode) and the thickness of PCM is 100 nm. The electrical characteristics were measured with Keithley 4200-SCS semiconductor characterization system, Keithley 4225-PMU ultra-fast I-V module, Keithley 4225-RPM remote amplifier/switch, and Keithley 3402 pulse/pattern generator. To stabilize the material in the programming area, we conducted dozens of the repeated operation between set and reset before the measurement to exactly measure electrical characteristics. The samples were annealed by rapid thermal annealing (RTA) process and the diffraction patterns of the annealed thin films were obtained with X-ray diffractometer. Bright-field transmission electron microscopy (BFTEM) and HRTEM analysis was conducted using FEI TITAN at 300 kV. The samples were annealed by RTA process at 450 °C for 30 min and prepared by mechanical polishing.

3. Results and discussion

3.1. Doping formation energy and distortion angle at each site

Table I shows values of changed formation energy and distorted angle by 29 elements. The computational high-throughput method calculates the changed stability by substitutional dopants with formation energy calculation using Eq. (1). Twenty-nine dopants (Ag, Bi, Co, Cr, Er, Fe, Ga, Gd, Ir, Po, Rh, Ge, Ta, Nb, Sc, Zr, Mo, Si, La, Lu, Tl, V, Pr, Tb, Y, Yb, Cu, Ti, and Zn) are chosen since these elements are generally used in the semiconductor industry. The computational high-throughput calculation can be used to obtain the information whether the dopants substitute the host atoms or not. Doping formation energy means the thermal stability of 29 dopants when the dopant replaces the host atoms among In, Sb, and Te in the IST atomic structure. The sign of the formation energy is the stability after doping. The negative value means stable at the site, on the other hand, the positive value means unstable at the site, resulting in the phase separation and element segregation while phase-change is countlessly repeated. For your information, the doping formation energies for some elements of above 29 elements were also calculated as interstitial atom. However, as the results can be expected, the values have no meaning because they are too high.

In a previous study,[32] we considered only four elements (Y, Gd, Bi, and La) having negative value of the doping formation energy as the adequate candidates. The reason why we report all the data in this paper is that some elements with a positive value of the doping formation energy may be qualified as good dopants. In addition, doping with over two elements of 29 elements can make the novel materials that are not yet known. The values of doping formation energy and distortion angle must be very important information to easily and faster develop novel materials, but the values of doping formation energy does not involve the temperature and entropy terms. In other words, the Gibbs free energy (ΔG) can be considered instead of the change of the enthalpy (ΔH). The entropy is expressed using Stirling formula:

$$\ln(N!) \approx N \cdot \ln N - N, \tag{2}$$

it can be simply expressed to

$$S_{\text{conf}} = -k_{\text{B}} \cdot [x_a \ln x_a + x_b \ln x_b + \cdots + (1 - x_a - x_b - \cdots)\ln(1 - x_a - x_b - \cdots)], \tag{3}$$

where k_{B} is the Boltzmann constant, x is the fraction of each element (a, b, …) in the material.

For example, when a certain element is doped with 10% at Sb site in IST, the value of changed entropy (ΔS) is $-5.12\ \mu\text{eV K}^{-1}\ \text{atom}^{-1}$. Interestingly, if a certain element is doped with 10% at In site, ΔS is $-18.3\ \mu\text{eV K}^{-1}\ \text{atom}^{-1}$. Although the value of enthalpy is larger than that of entropy, the $T\Delta S$ can influence on the total energy at high temperature. In addition, when the dopant substitutes at In site, the effect of entropic value increases over three times. From this result, more dopants near zero as well as four dopants (Gd, La, Y, and Bi) become promising candidates for IST, and number of cases to discover novel materials increases.

In our previous studies,[31,40] it was demonstrated that yttrium and bismuth were doped at In and Sb sites, respectively. The concentrations of Y-IST and Bi-IST were 12.38 at%Y and 5.5 at%Bi in IST material, and the electrical characteristics for operation speed of the doped devices were quite faster than that of pure IST device. The important fact through comparison between previous studies and this result is the relationship between the concentration limit and the

Table I. Calculated doping formation energy and distortion angle at each site.

Dopant	Doping formation energy (eV/atom)			Lattice distortion angle (degree)		
	In site	Sb site	Te site	In site	Sb site	Te site
Ag	2.42[a)]	2.61	3.41	2.51	1.24	1.13
Bi	1.84	−0.36[a)]	2.41	2.21	2.28	0.98
Co	2.30[a)]	4.24	4.50	2.91	8.23	13.98
Cr	2.77[a)]	4.14	5.14	2.50	33.22	16.90
Er	0.20[a)]	2.51	3.56	1.49	1.24	2.22
Fe	3.29[a)]	6.02	7.13	1.61	1.09	1.56
Ga	1.91[a)]	2.33	3.24	2.20	0.54	1.34
Gd	−0.80[a)]	6.89	8.57	1.58	1.19	2.81
Ir	1.87[a)]	3.59	3.95	1.94	6.47	16.95
Po	1.95	1.11[a)]	1.88	2.57	1.29	2.87
Rh	1.54[a)]	2.72	3.46	2.31	35.35	16.62
Ge	6.87[a)]	7.22	8.00	6.45	4.27	3.45
Ta	3.38[a)]	6.22	7.34	7.36	23.66	2.91
Nb	3.01[a)]	5.56	6.53	3.31	1.95	12.23
Sc	0.56[a)]	1.40	2.21	4.11	28.82	30.54
Zr	1.20[a)]	3.94	5.10	12.4	23.84	1.08
Mo	3.58[a)]	4.36	4.93	6.58	18.86	20.87
Si	2.58[a)]	2.97	3.66	5.21	4.14	6.90
La	−0.15[a)]	1.82	3.32	1.90	28.62	14.07
Lu	0.34[a)]	2.57	3.59	1.62	18.43	39.26
Tl	1.86[a)]	2.06	3.05	1.44	1.98	2.25
V	2.78[a)]	4.82	6.95	6.17	21.59	24.27
Pr	0.04[a)]	3.30	4.48	1.33	0.24	1.14
Tb	0.15[a)]	1.23	1.99	2.22	44.50	32.32
Y	−0.57[a)]	2.10	3.01	1.98	23.65	30.74
Yb	3.81	2.14[a)]	3.37	0.55	2.16	2.73
Cu	0.66[a)]	1.22	2.02	4.4	10.59	1.49
Ti	1.98[a)]	2.26	3.31	4.37	8.34	26.69
Zn	2.36[a)]	2.64	3.52	2.99	1.94	2.37

a) Marked values indicate the lowest doping formation energy and the site.

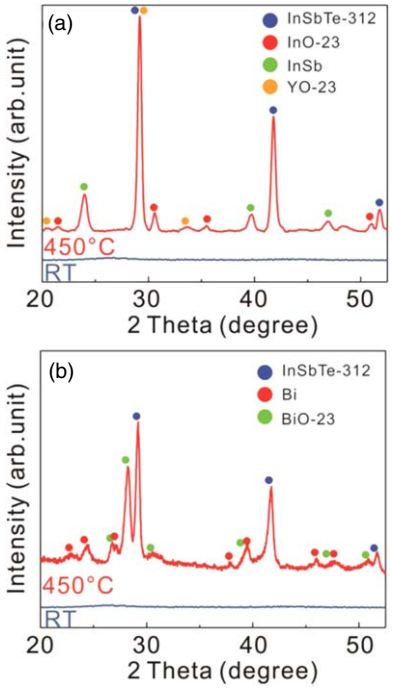

Fig. 1. (Color online) X-ray spectra of (a) 18.22 at%Y-doped IST and (b) 10.8 at%Bi-doped IST. The as-deposited thin films are analyzed at room temperature and 450 °C for 30 min.

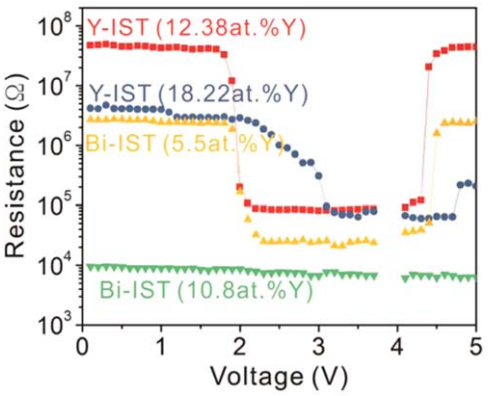

Fig. 2. (Color online) Electrical characteristics of Y-doped and Bi-doped IST. From 0.1 to 3.7 V, rise and fall time of electrical pulse are 100 ns. From 4.0 V to 5.0 V, rise and fall time of electrical pulse are 100 ns and 5 ns, respectively.

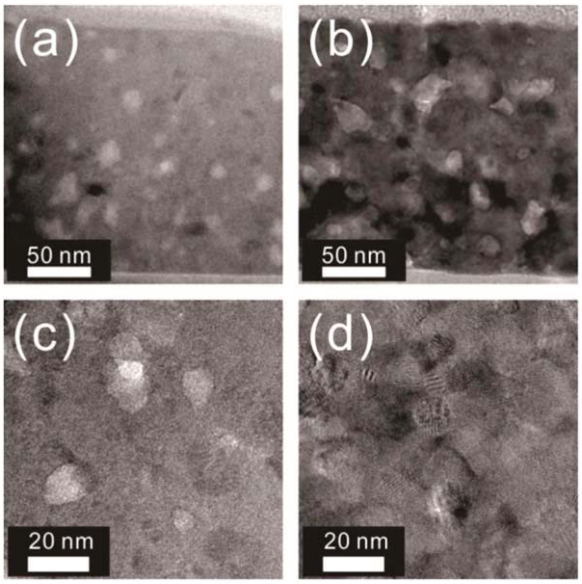

Fig. 3. (Color online) BFTEM and HRTEM images of (a), (c) 18.22 at%Y-doped IST and (b), (d) 4.18 at%Y-doped IST thin films at 450 °C and 30 min.

doping site of host sites. Figure 1 shows the peaks of X-ray diffraction at room temperature and 450 °C. When Y atoms were doped with 12.38 at% in IST, the phase is stably transited to crystalline Y-IST, on the other hand, the phase transition of 18.22 at%Y-doped IST is not completed to crystalline IST phase at 450 °C. It means that all of doped Y atoms are not easy to substitute the Sb atoms and disturb the phase transition to stable phase. The excessive yttrium atoms delay the phase transition and InSb phase remains with yttrium oxide formed by oxidizing no substituted yttrium atoms. Likewise, in case of 10.8 at%Bi-doped IST, it is shown that the doped Bi atoms cannot perfectly substitute Sb sites. The Bi atoms which are not substituted in IST structure are oxidized as bismuth oxide (Bi_2O_3). In fact, the concentrations of In and Sb in IST are 50% and 16.7%, respectively. All host atoms should be substituted by doped element. From above result, it can be confirmed that the number of In site is the greatest number among In, Sb, and Te sites in IST, and the controllable range for In doping is wider than Sb and Te sites. Therefore, it can have more of an effect of property change with doping at the In site.

Figure 2 shows electrical characteristics of Y-doped and Bi-doped IST according to composition change. These devices were measured after enough repeated switching to make stable programming region in the cell. From this figure, the device of Y-doped IST is well operated when the amount of Y atoms is 12.38 at%Y. The device of Bi-doped IST is also switched with large on/off ratio between amorphous and crystalline states. However, in both cases, the materials with excessive doping concentration cannot be used as device. The reliability of operation, one of the most important factors for device applications, is satisfied as shown in Fig. 2. This implies that when a certain dopant is added in IST, the reliability for switching of device is reduced by excessive dopant. Yttrium and bismuth atoms of 12.38 at%Y and 5.5 at%Bi substitute at In sites and Sb sites with removing In and Sb atoms, respectively. The portion of In and Sb sites in IST material is 50% and 16.7%. The 12.38 at%Y and 5.5 at%Bi occupy about 25% of In sites and 30% of Sb sites in IST material. In other words, the doping process should be performed with below 30% of the substitutional site.

Figure 3 shows the comparison between 18.22 at%Y-doped IST and 4.18 at%Y-doped IST thin films using TEM. From the two thin films with large difference in concentration of Y, it is definitely showed that the crystallization of 4.18 at%Y-doped IST is uniformly formed across the thin film, and there are more grains in Fig. 3(d), compared with those in Fig. 3(d). However, 18.22 at%Y-doped IST thin film looks like mixture phases which might consist of crystalline and amorphous phases as mentioned above Fig. 1. The amorphous phase is assumed to consist of indium oxide and amorphous InTe, in addition, the crystalline phase is presumed to be InSb, IST, and yttrium oxide. Therefore, at the same annealing condition, excessive dopants clearly interfere with the general phase transition from the amorphous to stable crystalline phases.

4. Conclusions

In conclusion, all doping formation energy values and distortion angles for the IST material are reported in this study. The data gives important information in helping to develop novel PCMs with more than two dopants as well as only one dopant in IST material. In addition, experimental results through XRD, TEM, and electrical measurements demonstrate that excessive dopants delay the stable phase transition and lower reliability of materials. It is implied that the maximum amount of dopant should be below 30% of each substitutional site. Therefore, the results will provide information about dopants and the way to develop novel materials with considerations.

Acknowledgments

This work has been supported by Korea Institute of Science and Technology (Grant No. 2E28000 and 2E28070). H. C. was supported by "Make Our Planet Great Again—German Research Initiative (MOPGA-GRI)" project fund of DAAD.

1) R. Jeyasingh, S. W. Fong, J. Lee, Z. Li, K.-W. Chang, D. Mantegazza, M. Asheghi, K. E. Goodson, and H.-S. P. Wong, Nano Lett. **14**, 3419 (2014).
2) D. Loke, T. Lee, W. Wang, L. Shi, R. Zhao, Y. Yeo, T. Chong, and S. Elliott, Science **336**, 1566 (2012).
3) M. Wuttig and N. Yamada, Nat. Mater. **6**, 824 (2007).
4) M. Wuttig, Nat. Mater. **4**, 265 (2005).
5) M. Cassinerio, N. Ciocchini, and D. Ielmini, Adv. Mater. **25**, 5975 (2013).
6) Y. Lu, S. Song, Y. Gong, Z. Song, F. Rao, L. Wu, B. Liu, and D. Yao, Appl. Phys. Lett. **99**, 243111 (2011).
7) C. Kim, D. Kang, T.-Y. Lee, K. H. Kim, and Y.-S. Kang, Appl. Phys. Lett. **94**, 193504 (2009).
8) S. Raoux, R. M. Shelby, J. Jordan-Sweet, B. Munoz, M. Salinga, Y.-C. Chen, Y.-H. Shih, E.-K. Lai, and M.-H. Lee, Microelectron. Eng. **85**, 2330 (2008).
9) M. Longo et al., J. Cryst. Growth **310**, 5053 (2008).
10) M. Wuttig, D. Lusebrink, D. Wamwangi, W. Welnic, M. Gillessen, and R. Dronskowski, Nat. Mater. **6**, 122 (2007).
11) G. W. Burr et al., IEEE J. Emerg. Sel. Top. Circuits Syst. **6**, 146 (2016).
12) N. Takaura, M. Kinoshita, M. Tai, T. Ohyanagi, K. Akita, and T. Morikawa, Jpn. J. Appl. Phys. **54**, 04DD01 (2015).
13) D. H. Shin, M. J. Song, J. W. Kim, G. H. Kim, K. Hong, and D. S. Lim, Jpn. J. Appl. Phys. **53**, 031402 (2014).
14) X. N. Cheng, F. X. Mao, Z. T. Song, C. Peng, and Y. F. Gong, Jpn. J. Appl. Phys. **53**, 050304 (2014).
15) J. H. Los, T. D. Kühne, S. Gabardi, and M. Bernasconi, Phys. Rev. B **88**, 174203 (2013).
16) E. T. Kim, J. Y. Lee, and Y. T. Kim, Phys. Status Solidi RRL **3**, 103 (2009).
17) C. S. Kim, J. Y. Lee, and Y. T. Kim, Appl. Phys. Lett. **100**, 151903 (2012).
18) V. L. Deringer, W. Zhang, P. Rausch, R. Mazzarello, R. Dronskowski, and M. Wuttig, J. Mater. Chem. C **3**, 9519 (2015).
19) T. Matsunaga, J. Akola, S. Kohara, T. Honma, K. Kobayashi, E. Ikenaga, R. O. Jones, N. Yamada, M. Takata, and R. Kojima, Nat. Mater. **10**, 129 (2011).
20) M. Salinga, E. Carria, A. Kaldenbach, M. Bornhofft, J. Benke, J. Mayer, and M. Wuttig, Nat. Commun. **4**, 2371 (2013).
21) X. Shen, Y. Chen, Z. Wang, Y. Lu, and S. Dai, Appl. Phys. A **119**, 425 (2015).
22) C. Peng et al., Appl. Phys. Lett. **101**, 122108 (2012).
23) S. K. Pandey and A. Manivannan, Appl. Phys. Lett. **108**, 233501 (2016).
24) G. Wang, Q. Nie, X. Shen, R. Wang, L. Wu, J. Fu, T. Xu, and S. Dai, Appl. Phys. Lett. **101**, 051906 (2012).
25) G. Torricelli, P. J. van Zwol, O. Shpak, G. Palasantzas, V. B. Svetovoy, C. Binns, B. J. Kooi, P. Jost, and M. Wuttig, Adv. Funct. Mater. **22**, 3729 (2012).
26) J. Orava, A. Greer, B. Gholipour, D. Hewak, and C. Smith, Nat. Mater. **11**, 279 (2012).
27) M. H. Jang, S. J. Park, D. H. Lim, S. J. Park, M.-H. Cho, D.-H. Ko, M. Heo, H. C. Sohn, and S.-O. Kim, Appl. Phys. Lett. **96**, 052112 (2010).
28) D. Lencer, M. Salinga, B. Grabowski, T. Hickel, J. Neugebauer, and M. Wuttig, Nat. Mater. **7**, 972 (2008).
29) X. Ji, L. Wu, M. Zhu, F. Rao, Z. Song, Z. Hu, S. Guo, L. Xu, X. Zhou, and S. Feng, RSC Adv. **5**, 24966 (2015).
30) M. Wuttig, D. Lüsebrink, D. Wamwangi, W. Wełnic, M. Gilleßen, and R. Dronskowski, Nat. Mater. **6**, 122 (2006).
31) M. Choi, H. Choi, S. Kim, J. Ahn, and Y. T. Kim, Sci. Rep. **5**, 12867 (2015).
32) M. Choi, H. Choi, S. Kwon, S. Kim, K.-R. Lee, J. Ahn, and Y. T. Kim, Int. Conf. on Solid State Devices and Materials (SSDM2018), 2018, p. 897.
33) M. Choi, H. Choi, S. Kim, J. Ahn, and Y. T. Kim, J. Korean Phys. Soc. **71**, 946 (2017).
34) W. Kohn and L. J. Sham, Phys. Rev. **140**, A1133 (1965).
35) J. Ihm, A. Zunger, and M. L. Cohen, J. Phys. C: Solid State Phys. **12**, 4409 (1979).
36) J. P. Perdew, J. Chevary, S. Vosko, K. A. Jackson, M. R. Pederson, D. Singh, and C. Fiolhais, Phys. Rev. B **46**, 6671 (1992).
37) J. P. Perdew, K. Burke, and M. Ernzerhof, Phys. Rev. Lett. **77**, 3865 (1996).
38) G. Kresse and J. Hafner, Phys. Rev. B **47**, 558 (1993).
39) H. J. Monkhorst and J. D. Pack, Phys. Rev. B **13**, 5188 (1976).
40) M. Choi, H. Choi, S. Kwon, S. Kim, K. R. Lee, J. Ahn, and Y. T. Kim, Phys. Status Solidi RRL **11**, 1700275 (2017).